ACADEMIC PRESS

Available online at www.sciencedirect.com

SCIENCE DIRECT®

Journal of Sound and Vibration 263 (2003) 775–795

JOURNAL OF SOUND AND VIBRATION

www.elsevier.com/locate/jsvi

# Feedback control of sound transmission through a double glazed window

O.E. Kaiser[a,*,1], S.J. Pietrzko[b], M. Morari[a]

[a] *ETH—Swiss Federal Institute of Technology, Automatic Control Laboratory, CH-8092 Zurich, Switzerland*
[b] *EMPA—Swiss Federal Laboratories for Materials Testing and Research, CH-8600 Dubendorf, Switzerland*

Received 3 October 2001; accepted 10 May 2002

**Abstract**

One way to tackle the control of stochastic noise in three dimensions is to reduce the sound transmission to the zone of interest. In buildings, windows are often the weak link in protecting the interior from outside noise. In particular, double glazed windows have a poor sound insulation at low frequency around the mass–air–mass resonance (double wall resonance). Since passive means for windows are exhausted, an active controller that increases the transmission loss in the low-frequency range is an attractive approach to reduce the noise level in buildings. Previously suggested feedforward controllers need reference microphones to measure the disturbance outside and error microphones for the adaptation somewhere in the room. For a real window this is unpractical or even unfeasible. These limitations can be overcome with the feedback controller presented here, which only uses sensors and actuators in the cavity of the double glazed window. Four different controllers—two feedforward and two feedback strategies—are designed, implemented and compared. With feedback the noise transmission around the mass–air–mass resonance can be reduced by 13 dB, compared to 18 dB with a feedforward controller.


## 1. Introduction

Noise is perceived more and more as an environmental pollutant or stress factor, and attempts are made to reduce noise whenever possible. In buildings, windows are often the weak link in protecting the interior from the outside noise, and therefore double glazed windows are used which provide good noise insulation.

*Corresponding author. Tel.: +41-585-580711; fax: +41-585-545979.
*E-mail address:* oliver.kaiser@siemens.com (O.E. Kaiser).
[1] Current address: Siemens Switzerland Ltd., CH-8047 Zurich, Switzerland.

0022-460X/03/$ - see front matter 
doi:10.1016/S0022-460X(02)01259-2

However, also double glazed windows have a poor transmission loss at low frequency. In addition, at a certain frequency, there is a significant drop in the transmission loss. This drop was termed mass–air–mass resonance because the model for infinite panels suggests that at this frequency the two panels move out-of-phase [1] thus causing a poor transmission loss. Even though recent results showed that for finite panels the situation is more complex [2,3] this terminology is also used in this case.

Since all the passive means to increase the transmission loss around the mass–air–mass resonance are more or less used, an active controller that increases the transmission loss in this frequency range could be deviced. In Ref. [4] a feedforward controller for a double glazed window was built. Also in Refs. [5–7] where more general double panel structures are discussed the focus is on feedforward controllers. However, since a measurement of the incident noise is often not available or impractical, in these circumstances a feedback scheme as suggested in Refs. [8,9] must be used.

The work presented here is a continuation and extension of Ref. [9] and is based on Ref. [10]. Section 3 derives a modal model of a double panel structure. After its successful validation this model is then used in Section 5 for the analysis of the structure and optimization of the sensor and actuator positions. After designing and implementing two feedforward controllers in Section 6, two feedback designs are presented in Section 7.

## 2. The experimental set-up

The experimental set-up consists of two rooms, the sending room where the noise source is, and the receiving room where the observer is (Fig. 1). The receiving room is a semi-anechoic chamber with oblique walls and a volume of 78.1 $m^3$. Furthermore, some damping panels were placed in the room to smooth the room response.

The double panel structure under study was installed in the wall opening between the two rooms. The panes themselves are monolithic glass panels with a size of $717 \times 1091$ mm. The pane on the transmission room side has a nominal thickness of 6 mm, the one on the receiving room side of 6 mm or 3.2 mm. The panel on the sending room side will be called *panel 1*, the other one *panel 2*. The set-up with the pane of 6 mm as panel 2 will be termed *symmetric configuration*, the one with the pane of 3.2 mm as panel 2 will be named *asymmetric configuration*.

The double panel was mounted in wooden sashes with dimensions $x = 1480$ mm and $y = 1230$ mm (Fig. 1). These sashes consist of an inner frame and an outer frame on each side. The outer frame can be removed, so that the pane can be exchanged. On the inside there are rubber edges which press on the glass once the outer frame has been tightened. The cavities inside the sashes were filled with several layers of damping material.

The interpanel spacing of 84 mm was filled with air. This unusually large spacing was chosen to simplify the mounting of control speakers in the cavity (Fig. 2). In addition to the speakers, microphones were mounted in the cavity between the panels.

To evaluate the performance, a hemispheric array with nine microphones was used. The microphones were held in place with thin wire (Fig. 1).

For the data acquisition, the measurements and the controller implementation, a Pentium II PC with 450 MHz was used. The data IO was carried out with two PCI-MIO-16E-4 cards from

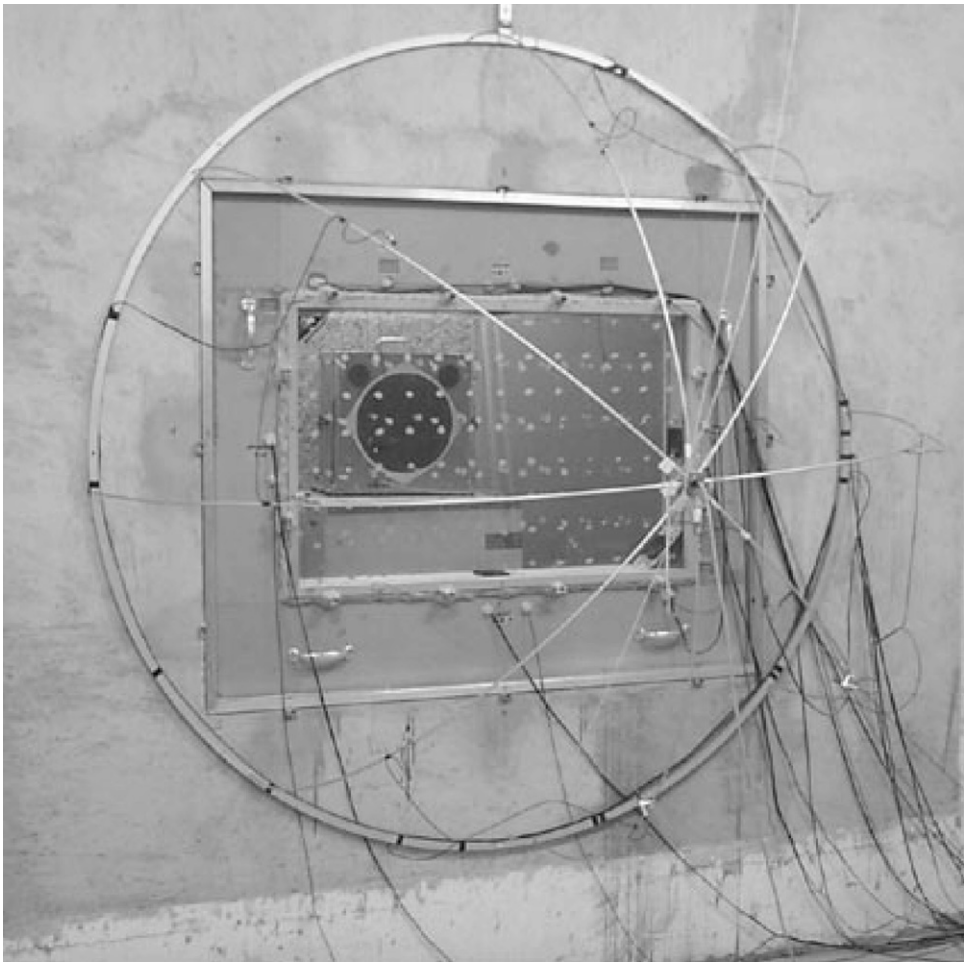

Fig. 1. View of the experimental set-up at EMPA. The panes are mounted in wooden sashes to fit in the opening between the transmission and the receiving room. The cables connect the microphones and speakers in the cavity with the amplifiers. A hemisphere with radius $r = 1$ m was built around the window on the receiving side. One microphone is located in the centre of the hemisphere. Eight microphones are located in a circle at 45° from the window.

National Instruments. All the experiments were implemented using the Real-Time Workshop from Matlab.

## 3. Modelling

For the modelling, a double panel structure was divided into five subsystems, namely the excitation dynamics, the first panel, the cavity, the second panel, and the radiation. Each subsystem is relatively well understood [11,12] and can be modelled with a modal approach. The models of the subsystems can then be assembled into a model of the double panel structure as

Fig. 2. Control speaker in the cavity between the panes. A microphone is mounted adjacent to the speaker.

suggested in Ref. [6]. Alternatively, the modelling could be performed using a finite element model as in Ref. [7]. It was decided to develop the model using a modal approach, because a modal model is well suited for analysis.

### 3.1. The panels

The motion of a thin rectangular, orthotropic plate with side lengths $a$ and $b$ is governed by the partial differential equation (PDE) [12]

$$K\left(\frac{\partial^4}{\partial x^4}+2\frac{\partial^4}{\partial x^2\,\partial y^2}+\frac{\partial^4}{\partial y^4}\right)w(x,y,t)+\rho h\frac{\partial^2}{\partial t^2}w(x,y,t)=-p(x,y,t), \tag{1}$$

where $w(x,y,t)$ is the displacement of the plate in the $z$ direction, $p(x,y,t)$ a pressure distribution on the surface, and $K$ a material constant [12,10]. In Ref. [13], a large number of other, more detailed models for plates are given. However, Eq. (1) proved to be sufficient for many practical cases [12].

Assuming simply supported boundary conditions and using a modal approach $w$ becomes

$$w(x,y,t) = \sum_{m=1}^{\infty} \sum_{n=1}^{\infty} w_{mn}(t)\Phi_{mn}(x,y), \tag{2}$$

where

$$\Phi_{mn}(x,y) = \sin\frac{m\pi x}{a}\sin\frac{n\pi y}{b} \tag{3}$$

is the $(m,n)$th mode shape function and $w_{mn}(t)$ is the corresponding instantaneous amplitude. It can be determined from the ordinary differential equation (ODE)

$$\ddot{w}_{mn}(t) + 2\zeta_{mn}\omega_{mn}\dot{w}_{mn}(t) + \omega_{mn}^2 w_{mn}(t) = -p_{mn}(t), \tag{4}$$

where the forcing term $p_{mn}$ is the projection of $p$ on the $(m,n)$th mode

$$p_{mn}(t) = \frac{1}{V_{mn}}\int_F \Phi_{mn}(x,y)p(x,y,t)\,\mathrm{d}F, \tag{5}$$

with $V_{mn}$ defined by

$$\int_F \Phi_{mn}\Phi_{pq}\,\mathrm{d}F = \begin{cases} V_{mn}, & m=p, n=q, \\ 0, & \text{otherwise.} \end{cases} \tag{6}$$

### 3.2. The cavity

The pressure in the cavity is governed by the acoustical wave equation [14]

$$\Delta p - \frac{1}{c^2}\ddot{p} = q, \tag{7}$$

where $q$ is a source distribution. Under the assumption of hard boundaries and with a modal approach

$$p(x,y,z,t) = \sum_{n=1}^{\infty} P_n(t)\Psi_n(x,y,z), \tag{8}$$

with the mode shapes

$$\Psi_n = \Psi_{ijk} = K_{ijk}\cos\frac{i\pi x}{a}\cos\frac{j\pi y}{b}\cos\frac{k\pi z}{d}, \quad i,j,k = 0,1,2,\ldots, \tag{9}$$

where $a$, $b$, and $d$ are the dimensions of the cavity in the $x$, $y$, and $z$ directions. As in the panel case, this infinite series can be truncated to a finite sum, and $P_n$ determined from the ODE

$$\ddot{P}_n + 2\delta_n\dot{P}_n + \omega_n^2 P_n = \frac{\rho c^2}{V_n}F_n(t), \tag{10}$$

where the damping term $2\delta_n\dot{p}_n$ and the forcing term on the right-hand side have been added [14]. The coefficient $V_n$ is the mode normalization factor given by

$$\int_V \Psi_m\Psi_n\,\mathrm{d}V = \begin{cases} 0, & m \neq n, \\ V_n, & m = n, \end{cases} \tag{11}$$

and $F_n(t)$ the modal force given by [14]

$$F_n(t) = \int_V \frac{\dot{Q}}{V} \Psi_n \, \mathrm{d}V - \int_S \ddot{w} \Psi_n \, \mathrm{d}S. \tag{12}$$

The first term describes the sources in the cavity and $Q$ is the volume velocity of these sources. The second term is due to the flexible walls and $\ddot{w}$ is the acceleration of the boundaries. Both terms can again be interpreted as projections on the $n$th cavity mode.

### 3.3. Coupling of the panels and the cavity

The pressure in the cavity drives the panels. Inserting Eq. (8) into Eq. (5), gives

$$p_{mn}(t) = \frac{1}{V_{mn}} = \sum_n P_n(t) S_{mn}, \tag{13}$$

where the coupling factor $S_{mn}$ is

$$S_{mn} = \int_S \Phi_m \Psi_n \, \mathrm{d}S. \tag{14}$$

Analogously, the effect of the panels on the cavity can be calculated from the second term in Eq. (12) as

$$F_n(t) = -\int_S \ddot{w} \Psi_n \, \mathrm{d}S = -\sum_m \ddot{w}_m(t) S_{mn}, \tag{15}$$

where the same coupling factors as in Eq. (13) enter the equation.

### 3.4. The speakers

Since the speakers are radiating into a cavity where the cavity pressure strongly interacts with the speakers, they need special consideration. As can be seen from Fig. 3, for the membrane of a speaker the following equation of motion holds [15,16]:

$$m_C \ddot{x} = A(p_R - p_F) + F_S - F_C. \tag{16}$$

The meaning of the different quantities is given in Table 1. The underlying assumptions are that the pressure is constant over the entire area of the membrane and that the membrane is stiff for the frequencies under consideration.

The restoring force $F_C$ can be modelled as a spring, i.e.,

$$F_C = k_C x + c_C \dot{x}. \tag{17}$$

Furthermore, the driving force $F_S$ of the speaker is generated by a voice coil (Fig. 4), i.e.,

$$L \frac{\mathrm{d}i}{\mathrm{d}t} = u - e - iR, \tag{18}$$

where

$$F = k_1 i, \tag{19}$$

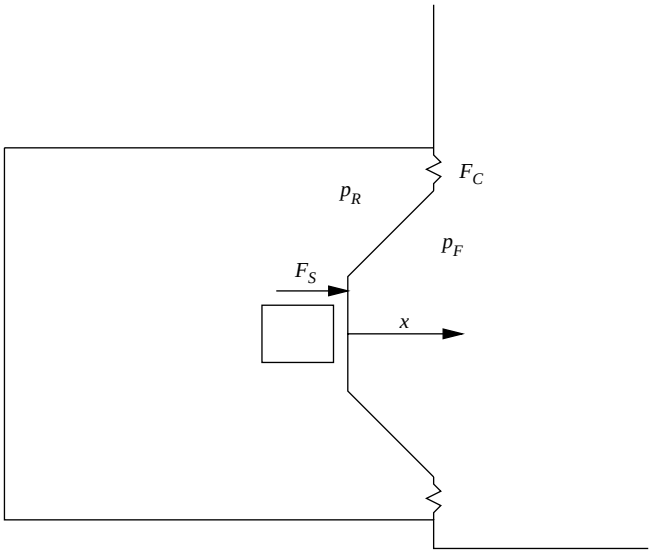


Fig. 3. A speaker membrane can be modelled as a rigid body driven by a force $F_S$ generated by a DC-motor, and affected by the front pressure $p_F$, the back pressure $p_R$, and the restoring force $F_C$ from the resilient mounting of the membrane.

Table 1
Parameters of the speakers

| Symbol | Meaning |
|---|---|
| $m_C$ | Mass of the speaker cone |
| $A$ | Area of the cone/piston |
| $p_R$ | Pressure on rear side |
| $p_F$ | Pressure on front side |
| $F_S$ | Driving force from the voice coil |
| $F_C$ | Force from the spring that keeps the cone in place |
| $R$ | Resistor of amplifier and voice coil |
| $L$ | Inductance of voice coil |
| $k_1$, $k_2$ | Coupling factors |
| $u$ | Voltage from amplifier |

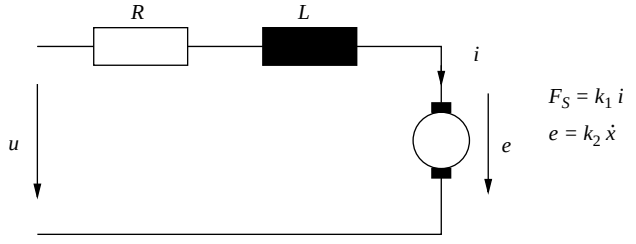


Fig. 4. Model of the voice coil of the speaker.

and

$$e = k_2 \dot{x}. \tag{20}$$

Due to reciprocity in transducers $k_1$ equals $k_2$. The above equations can be collected into a system as

$$\begin{bmatrix} \dot{x} \\ \ddot{x} \\ \frac{\mathrm{d}i}{\mathrm{d}t} \end{bmatrix} = \begin{bmatrix} 0 & 1 & 0 \\ -\frac{k_C}{m_C} & -\frac{c_C}{m_C} & \frac{k_1}{m_C} \\ 0 & -\frac{k_2}{L} & -\frac{R}{L} \end{bmatrix} \begin{bmatrix} x \\ \dot{x} \\ i \end{bmatrix} + \begin{bmatrix} 0 & 0 \\ \frac{A}{m_C} & -\frac{A}{m_C} \\ 0 & 0 \end{bmatrix} \begin{bmatrix} p_R \\ p_F \end{bmatrix} + \begin{bmatrix} 0 \\ 0 \\ \frac{1}{L} \end{bmatrix} u. \tag{21}$$

On the rear side, the membrane radiates into a small cavity of approximately $(0.08, 0.08, 0.10)$ m. Because the first mode $(0, 0, 1)$ is at 2706 Hz, it is justified to consider just the Helmholtz mode, i.e., the static pressure in the rear cavity. Hence,

$$p_R = -\frac{\gamma p_0 A}{V_0} x + o(x^2), \tag{22}$$

where $p_0$ is the pressure in the cavity for $x = 0$, $V_0$ the volume of the cavity, and $\gamma = 1.4$ is a constant (cf., Ref. [15] for details).

This leads to the system

$$\begin{bmatrix} \dot{x} \\ \ddot{x} \\ \frac{\mathrm{d}i}{\mathrm{d}t} \end{bmatrix} = \begin{bmatrix} 0 & 1 & 0 \\ -\frac{k_C}{m_C} - \frac{\gamma p_0 A^2}{m_C V_0} & -\frac{c_C}{m_C} - \frac{c_R}{m_C} & \frac{k_1}{m_C} \\ 0 & -\frac{k_2}{L} & -\frac{R}{L} \end{bmatrix} \begin{bmatrix} x \\ \dot{x} \\ i \end{bmatrix} + \begin{bmatrix} 0 \\ -\frac{A}{m_C} \\ 0 \end{bmatrix} p_F + \begin{bmatrix} 0 \\ 0 \\ \frac{1}{L} \end{bmatrix} u, \tag{23}$$

where some damping $c_R$ due to the cavity on the rear side was added. The numerical values of the individual speaker parameters can be calculated based on Ref. [15] and the data sheet.

The pressure on the front side $p_F$ can be calculated from the modal pressure $P_n$. The coupling of the speaker to the cavity can be derived from Eq. (12).

### 3.5. Excitation and radiation

In Refs. [11,17–19], and [12, p. 236] two methods to calculate the sound power radiated by a vibrating structure are outlined. In one case an attempt to solve the Rayleigh integral is made, whilst in the other a calculation via the wave number transform is suggested. Both approaches lead to a quadratic form that represents the radiated sound power [12]. In Ref. [18] methods to derive a state space representation from this quadratic form are indicated. However, since that procedure involves fitting transfer functions to every element of an $n \times n$-transfer matrix where in our case $n \approx 80$ it was decided to replace these transfer functions by simple constants derived from the excitation and radiation dynamics at the mass–air–mass resonance. These constants are a good model within the limited frequency range of interest (cf., Ref. [10] for details).

### 3.6. State space model

The panels, the cavity, and the speakers are governed by a finite number of ODEs. These systems of ODEs can all be transformed into state space form. Using the previously mentioned

coupling terms, these sub-models were then assembled into one large state space model, which included also the radiation and excitation terms.

## 4. Validation of the model

Two methods were used to validate the model. First, the double panel was excited with a large speaker in the sending room and the vibration on the second panel was measured using a laser vibrometer. When the measured operating deflection shapes were compared with the mode shapes predicted by the model, not only the mode shapes themselves but also the resonance frequencies agreed very well. In Fig. 5, the measurement at 88.1 Hz is given, and in Fig. 6 the prediction from the model at 88.5 Hz (asymmetric configuration). Since such a mode with two peaks in phase cannot occur on a simple plate it can be concluded that in the model the coupling is also correct.

Some transfer functions from the speakers in the cavity to some microphones in the cavity and some accelerometers on the structure were then measured. Again, the measurement and the prediction agreed quite well (Figs. 7 and 8).

To avoid an accidental fit, two different windows were tested with the laser vibrometer and four configurations were used to compare the transfer functions. In all the cases the fit was similar as in Figs. 5–8.

## 5. Optimization of the system

The positions of the sensors and actuators were optimized based on a controllability criterion [20]. First the coupled model from Section 3 was transformed into diagonal form. Then the controllability Grammian $W_{C_i}$ of every coupled mode was calculated. The controllability of mode $i$ with two speakers is then

$$W_{C_i}^{total} = W_{C_i}^{(1)} + W_{C_i}^{(2)}. \tag{24}$$

As cost function, the weighted sum of the controllability of the individual modes was used:

$$J = \sum f_i \, W_{C_i}^{total}, \tag{25}$$

where the weight factors $f_i$ are

$$f_i = \begin{cases} r_i \cdot \alpha & \text{if mode } i \text{ is in the frequency range of interest,} \\ -r_i & \text{if mode } i \text{ is in the spillover prevention range,} \\ 0 & \text{if mode } i \text{ is above the spillover prevention range.} \end{cases} \tag{26}$$

Due to the area formula (cf., e.g., Ref. [21, p. 87]), feedback controllers amplify the modes just above the frequency range of interest, where the crossover frequency of the controller is. This effect is often called spillover. As pointed out in Ref. [22], it can be reduced by placing the actuators and sensors so that they do not couple to the modes in this band. Therefore, the

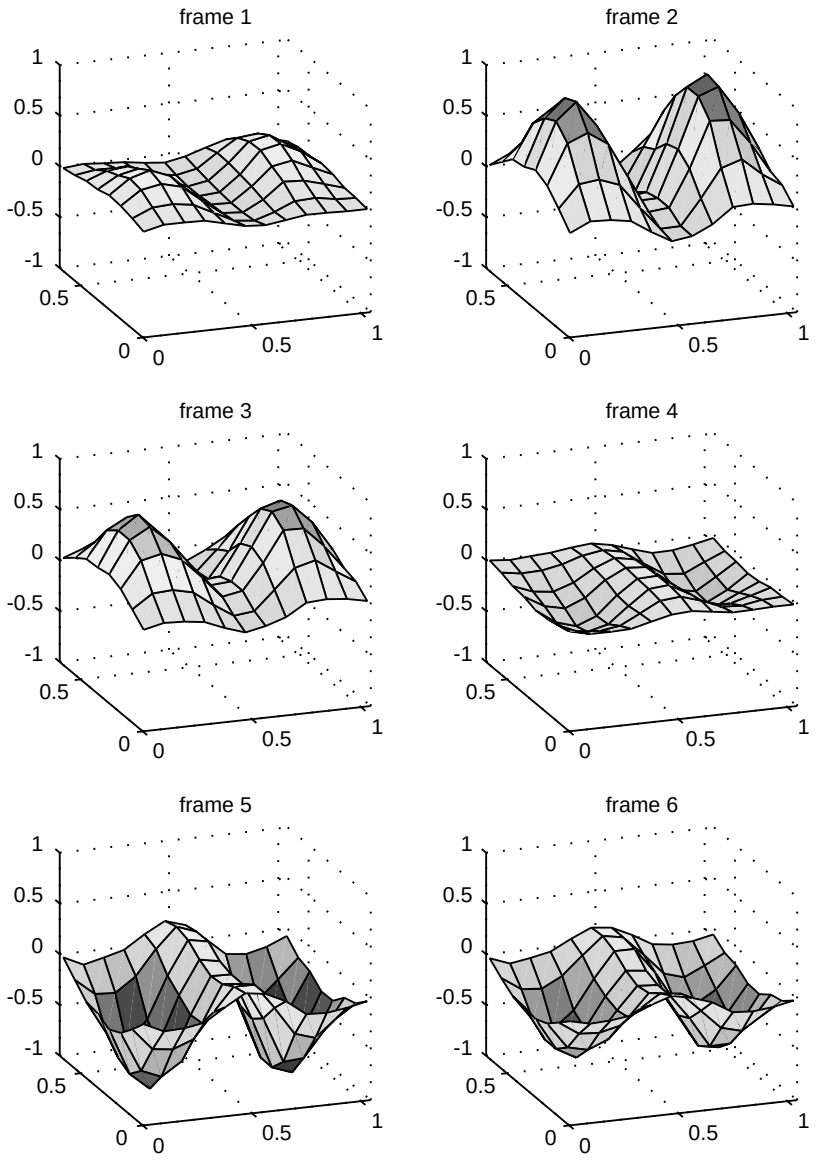


Fig. 5. Measured mode shape of panel 2 at 88.1 Hz. Asymmetric configuration: 6 mm pane, 84 mm cavity, 3.2 mm pane.

spillover prevention band of 100 Hz right above the frequency range of interest (40 Hz…200 Hz) was defined. The modes lying in this band entered the optimization with a negative sign, i.e., good controllability was punished.

The factor $r_i$ quantifies the radiation efficiency of mode $i$. For simplicity, it was set to the volume velocity of mode $i$ on the second panel. The factor $\alpha$ was varied from 1 to 2 to stress the

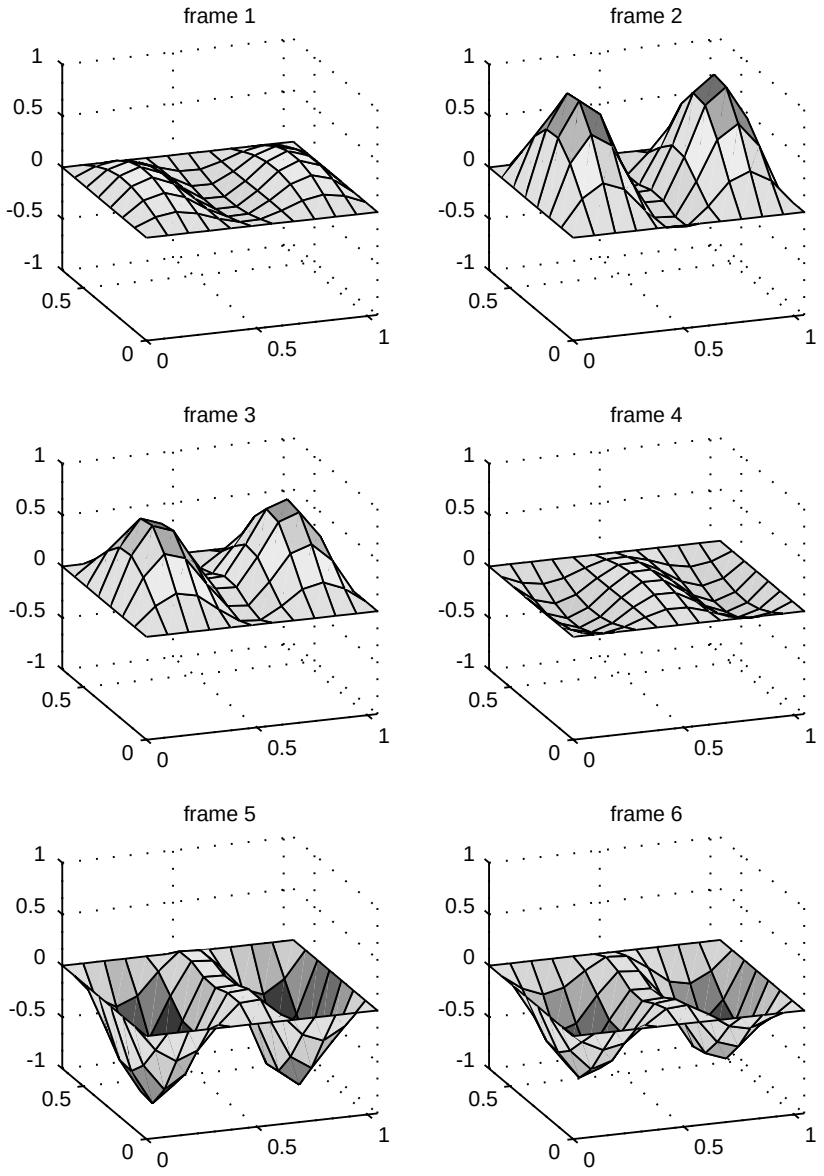


Fig. 6. Mode shape of panel 2 at 88.5 Hz as predicted from the model. Asymmetric configuration: 6 mm pane, 84 mm cavity, 3.2 mm pane.

controllability of the modes in the frequency range of interest versus the punishment of the modes in the spillover prevention band. Because the cost function is very cheap computationally the optimization was done by simple enumeration.

The optimization was performed for the symmetric and the asymmetric configuration and for different frequency ranges around the mass–air–mass resonance. The result indicated that three

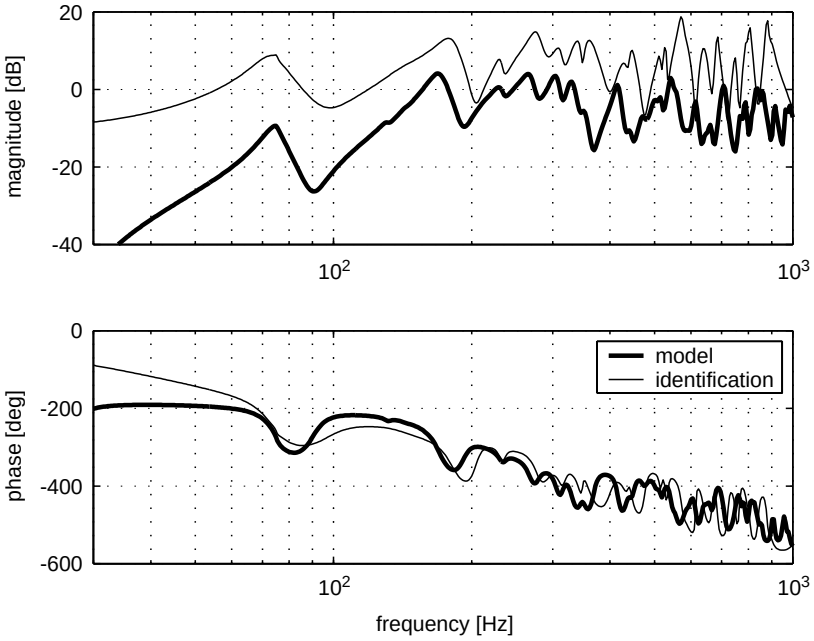


Fig. 7. Transfer function from the speaker in the lower right corner to a collocated microphone. Symmetric configuration: 6 mm pane, 84 mm cavity, 6 mm pane. The difference in gain is due to an unknown speaker parameter.

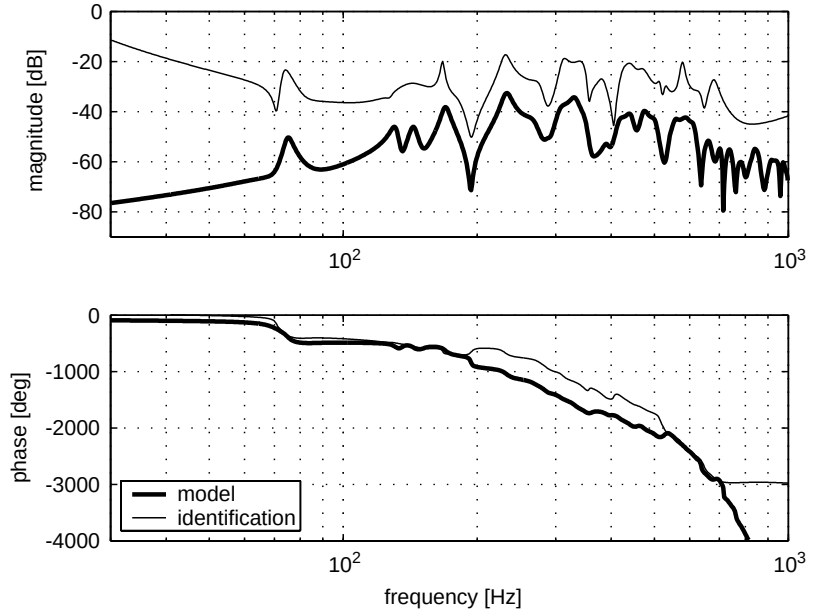


Fig. 8. Transfer function from the speaker in the lower right corner to an accelerometer at (0.94 m, 0.56 m) on panel 1. Symmetric configuration: 6 mm pane, 84 mm cavity, 6 mm pane. The difference in gain is due to an unknown speaker parameter.

speaker locations are superior: one speaker in the centre of the top and bottom boundary, one speaker in the centre of the left and right boundary, and two speakers in the corners.

Speakers were mounted in all the positions and control experiments were run for all three configurations. The differences in performance, however, were quite small. Apparently the optimum is quite flat and all three positions are reasonable.

## 6. Feedforward control

Feedforward controllers for double glazed windows or double panel structures in general have been studied before [4–7]. These controllers need an upstream measurement of the noise, e.g., with microphones somewhere outside, as a reference. For the adaptation, error microphones are necessary, which can be placed in the receiving room or in the cavity. Both the disturbance microphones outside and the error microphones in the receiving room are not very practical or are even unfeasible. Nevertheless, some feedforward experiments were performed in this study to get an upper bound of the performance achievable with a feedback controller.

In both the symmetric and the asymmetric configurations, two LMS-based feedforward controllers were implemented. For the former, the adaptation was based on the microphones in the receiving room, whereas the latter used the microphones in the cavity.

The largest attenuation was achieved for the asymmetric configuration with the error microphones in the receiving room. The attenuation near the mass–air–mass resonance was about 18 dB. The spectrum in the receiving room averaged over the microphones of the hemispheric array is given in Fig. 9.

If the microphones in the cavity are used as error microphones the performance of the controller at the mass–air–mass resonance deteriorates to 7.5 dB. Apparently, modal restructuring plays a more important role than modal suppression [7,6].

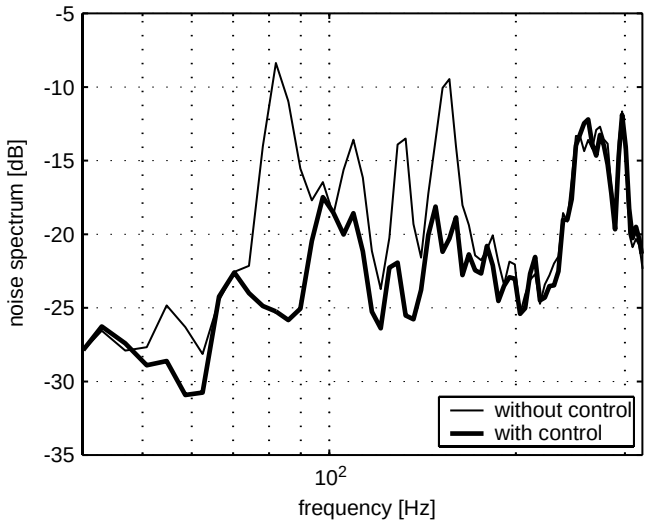


Fig. 9. The spectrum in the receiving room for controller 1 (asymmetric configuration).

Table 2
Performance comparison of the different controllers

| Controller | Symmetric panel (dB) | Asymmetric panel (dB) |
|---|---|---|
| 1. Feedforward controller with error microphones in the receiving room | 8.5 | 18 |
| 2. Feedforward controller with error microphones in the cavity | 4 | 7.5 |
| 3. IMC feedback controller | 7 | 13 |
| 4. Robust feedback controller | 4 | 7 |

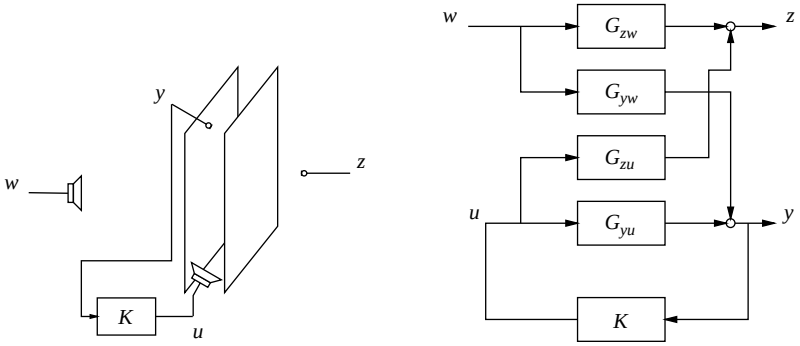


Fig. 10. The system has two sets of inputs, the disturbances $w$ and the control inputs $u$, and two sets of outputs, the internal microphones $y$ and the microphones in the receiving room $z$. Only the internal microphones and speakers are accessible for control (controller $K$).

The generally inferior performance of the symmetric panel (Table 2) can be explained by the uncontrollable modes. As pointed out in Ref. [23], some modes of the symmetrical configuration cannot be controlled with speakers in the cavity, which limits the achievable performance.

## 7. Feedback control

In Ref. [9] it was pointed out that installing a feedback controller according to Fig. 10 reduces to a so-called four-block design problem [24], i.e., to a design problem where the performance is specified on some quantities $w$ and $z$ which cannot be measured directly. Four-block problems have been studied for quite some time in control engineering literature and tools to solve them are available [25].

We want to minimize the (possibly weighted) transfer function $T_{zw}$ from $w$ to $z$, i.e.,

$$\min_K \|T_{zw}\| = \min_K \|G_{zw} + G_{zu}K(I - G_{yu}K)^{-1}G_{yw}\|. \tag{27}$$

The performance is not defined via some norm of a measurable system output but on a "computed" quantity. Of course, as an additional condition, $T_{zw}$ should be stable.

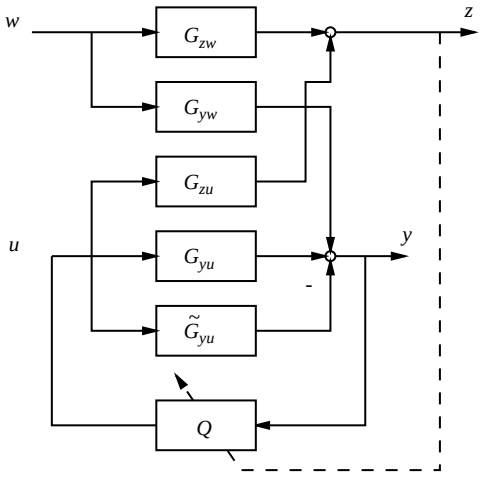


Fig. 11. With an LMS-based gradient design procedure an IMC controller was designed. After convergence the adaptation (dashed line) was turned off. The remaining system is a pure feedback scheme.

From the feedforward experiments described in the previous section it is clear that only a four-block design can be successful. If the controller was designed to minimize $y$, the achievable performance would be 7.5 dB compared to 18 dB in the four-block case.

Two feedback designs were tested: an IMC[2] controller based on the LMS-algorithm, and a controller designed with robust control tools. For easier reference the IMC controller will be called controller 3 and the robust design controller 4.

### 7.1. LMS-based IMC design

The driving force behind the LMS-based IMC design was the attempt to exploit the positive properties of the LMS-algorithm for feedback design. If feedforward controllers for stochastic noise are built, the cancellation signal can affect the disturbance measurement. For example, in a duct, the superimposed noise from the cancellation speaker can travel upstream to the disturbance microphone. A successful solution to this problem is to first design an echo canceller to get a better measurement of the disturbance and then to use the standard xLMS-algorithm to implement a feedforward controller [16]. Since this design procedure proved to be particularly well suited for vibrating plants, a similar feedback controller was developed.

Initially, the transfer function $G_{yu}$ from the control speakers to the control microphones in the cavity was identified with a finite impulse response filter (FIR) using the LMS-algorithm. Then the identified model $\tilde{G}_{yu}$ was used to compensate the plant as in Fig. 11, and an adaptive controller $Q$ based on the xLMS-algorithm was run. After 100 s the adaptation was "complete" and turned off. After turning off the adaptation this scheme is a pure feedback controller. (Fig. 11 without the dashed line.) The combination of $\tilde{G}_{yu}$ and $Q$ corresponds to an internal model control (IMC) controller [26] designed via a gradient optimization procedure.

[2] IMC: internal model control [26].

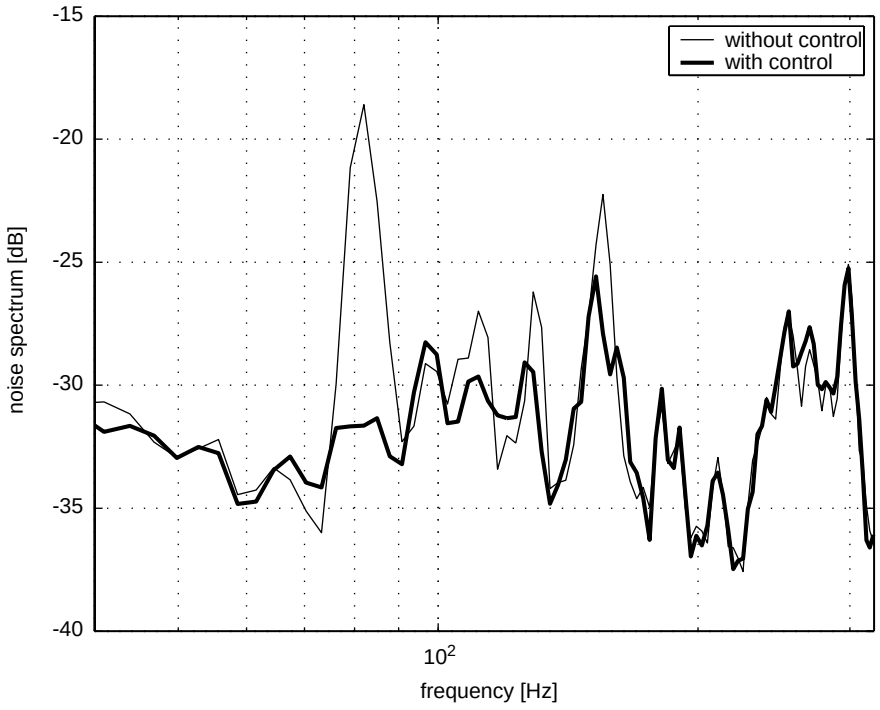


Fig. 12. Sound spectrum in the receiving room if the asymmetric double panel is controlled by the IMC controller (controller 3). The peak in the problematic area around 80 Hz is damped by 13 dB.

Different controller configurations were tested. After a series of trials a system with two reference microphones, one speaker, and two error microphones proved to work best (Fig. 12). The performance was as good as with two speakers, but there were no stability problems. With two speakers no reliable system could be built using the design procedure outlined. In many cases the controllers became unstable only a few seconds after turning off the adaptation. Without modification this approach seems to be unsuitable for multiple input multiple output (MIMO) design. As a consequence, a robust controller described in the next section was designed.

### 7.2. Robust controller design

The concept underlying the robust design framework is that a plant cannot be described by a single linear model. Therefore, the plant $P$ is characterized by a set

$$P = P_{nom} + W_1 \Delta W_2, \tag{28}$$

where $\Delta$ is an arbitrary, stable and norm-bounded transfer function,

$$\|\Delta\|_\infty < 1, \tag{29}$$

and $W_1(j\omega)$ and $W_2(j\omega)$ are weighting functions that are small where $P_{nom}$ is a good description of the real plant, and large for those frequencies where $P_{nom}$ is a poor model. The real plant is assumed to lie somewhere in this set. Accordingly, the modelling consists of two steps: the

derivation of the nominal model $P_{nom}$ and the uncertainty description $W_1$, $W_2$. For a more detailed introduction to the concept of uncertainty and alternative uncertainty descriptions Refs. [21,26], or Ref. [24] may be consulted.

In the robust control framework, controllers are not designed for one single nominal plant $P_{nom}$, but for the entire set $P$. Robust performance is only achieved if the performance specifications hold for all members of $P$. The advantage of this method is that it can cope with unmodelled dynamics which often leads to superior controllers, in particular for MIMO systems.

### 7.2.1. Identification for control

To design a controller with the robust control tools mentioned earlier, a nominal model which contains models for all four blocks of Fig. 10 and which is of low order must be found. In addition it should be continuous and in state space form because the software package [25] can handle these type of models only.

Based on the experience in Refs. [9,27] it was decided to use subspace identification [28], because it can fulfill all the conditions above except that the model is in discrete time. However, the transformation to continuous time is relatively straightforward using a Tustin transformation with pre-warping [29].

The disturbance and control inputs were excited simultaneously with band-limited white noise and all the microphones in the cavity and in the receiving room were recorded. After detrending and normalizing the data, and removal of some delays the four block model was identified in one single calculation using the subspace identification algorithm `n4sid` from Ref. [30].

### 7.2.2. Uncertainty description

As pointed out in the introductory remarks, in addition to the nominal model an uncertainty description for the plant is needed. However, since there is no systematic way to derive such an uncertainty description, some physical intuition was used.

The full model $G_{yu}$ from the speakers to the microphones is

$$G_{yu} = G_{yu}^{nom} + W_1 \Delta W_2, \tag{30}$$

where $G_{yu}^{nom}$ is the nominal model from the previous subsection. It is known that the speakers are fairly inefficient and the microphones more or less insensitive at low frequency. Therefore the identified model derived from real data cannot be accurate in this frequency range and the uncertainty $W_1$, $W_2$ should be large. Furthermore, there are some unmodelled modes at high frequency. Hence, in this area also a large uncertainty is necessary.

A stable filter that fulfills these conditions—high gain at low and high frequencies, small gain in the frequency range of interest—is a band-stop filter. Hence, the filter $W_2$ was chosen as a diagonal $2 \times 2$-transfer matrix with such band-stop filters on the diagonal. The magnitude of the pass band was chosen to be larger than the nominal model, whilst the magnitude of the stop band was smaller. To avoid the numerical problems associated with multiple poles [31], the cut-off frequencies of these two band-stop filters were chosen to be disparate. For simplicity, $W_1$ was chosen as an identity matrix. In Ref. [24] some interpretation of this and various other uncertainty descriptions is given.

The additive uncertainty in Eq. (30) is not the only possibility to describe uncertainty. As has been pointed out, for example in Ref. [27], the choice of the uncertainty model can be crucial for the performance. Ideally, only the uncertainty at low and high frequency is modelled as unstructured uncertainty whereas the one in the frequency range of interest is represented with parametric uncertainty [24,27]. However, for the system available a decomposition necessary for introducing parametric uncertainty is very cumbersome.

### 7.2.3. Controller optimization

The controller should focus on the frequency range of interest around the mass–air–mass resonance. This can be achieved by using a performance weight that is large exactly at these frequencies and small otherwise, e.g., a band-pass filter.

The interconnection of the nominal plant, the uncertainty and the performance weights (Fig. 13) is called the augmented system [24]. The actual controller design can be posed as a minimization problem on the augmented system. For robust performance, one has to find a $K$ such that the transfer function $T_{z\tilde{w}}$ from the disturbance $\tilde{w}$ to the performance signal $z$ is smaller than some specified constant $\gamma$ for all $\Delta$, i.e., find a $K$ such that

$$\max_{\Delta} \|T_{z\tilde{w}}\|_{\infty} < \gamma, \tag{31}$$

which is equivalent to

$$K = \arg \min_{K} \max_{\Delta} \|T_{z\tilde{w}}\|_{\infty}. \tag{32}$$

In Ref. [25] efficient tools to pose and solve Eq. (32) are given. The interested reader is referred to Ref. [24] for details about this procedure.

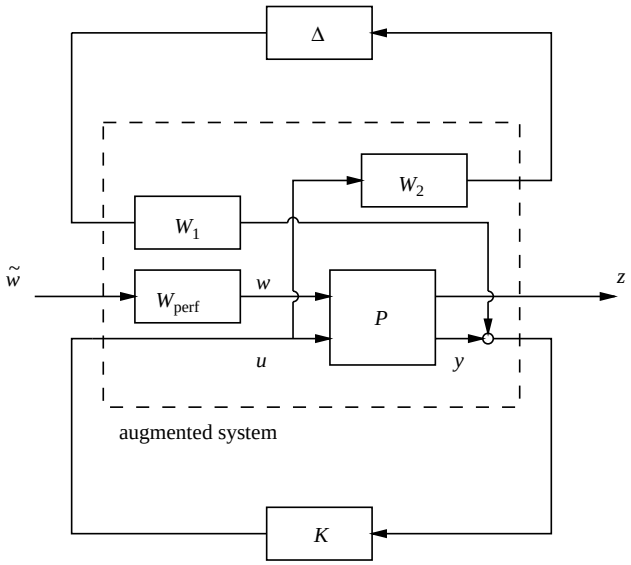


Fig. 13. Augmented system used for the controller optimization. The disturbance $\tilde{w}$ is weighted by $W_{perf}$. $W_1$ and $W_2$ are weights for the size of the uncertainty.

The identified system had 90 states. After eliminating some of the higher order modes and adding the weights, the augmented system had 98 states. Due to experience with systems of similar size [32] it was made sure that all the weights were minimum phase and balanced. After taking these precautions the $\mathscr{H}_\infty$-optimization encountered no numerical problems.

*7.2.4. Results*

The performance as well as the uncertainty weights were varied to get the best possible performance. For the asymmetric panel, the first resonance was attenuated by approximately 7 dB. For the symmetric panel, the reduction was 4 dB.

## 8. Conclusions

The transmission loss of double glazed windows can be increased with an active controller. Using feedback, no microphones outside the window are necessary, which improves the practicality of the system.

In Table 2, a performance comparison of all the controllers implemented on the double glazed window is given. As a performance index, the noise reduction in dB at the mass–air–mass resonance around 80 Hz is used. Of several controllers or speaker configurations tested, the best results were reported in Table 2. By comparing the entries, the following statements can be made:

- It is possible to build feedback controllers whose performance is almost as good as that from the feedforward controller. In particular, it is possible to build feedback controllers (controller 3) whose performance is superior to the feedforward controller with the error microphones in the cavity (controller 2) which confirms the necessity for a four-block design in this case.
- In general, the noise reduction is better for the asymmetric panel. Some modes of the symmetric panel are uncontrollable with speakers in the cavity which limits the performance. Therefore, windows with active controllers should be built asymmetrical.
- To some extent, the inferior performance of the robust design is due to the conservativeness introduced by the unstructured uncertainty model.
- The feedforward controller that uses the receiving room microphones is much better than the one that uses the microphones in the cavity. Apparently modal restructuring plays an important role and modal suppression is not sufficient for this set-up.

Future work could address the design of feedback controllers that combine the good properties of controller 3 and 4, namely good performance and robustness, by using more specific uncertainty descriptions as in Refs. [33,27].

## References

[1] L. Cremer, M. Heckl, Körperschall, Springer, Berlin, 1996.
[2] S.J. Pietrzko, Vibroacoustic behaviour of a double glazed window; modal testing and a model employing general parameters, in: Proceedings of Inter-Noise 96, 1996.

[3] S.J. Pietrzko, Tieffrequentes Schwingungsverhalten einer Doppelverglasung, in: Proceedings of Deutsche Jahrestagung für Akustik DAGA 98, Zurich, 1998.
[4] P. De Fonseca, W. Dehandschutter, P. Sas, H. Van Brussel, Implementation of an active noise control system in a double-glazing window, in: Proceedings of ISMA 21, Noise and Vibration Engineering Conference, Leuven, Vol. 1, 1996, pp. 377–388.
[5] C. Bao, J. Pan, Experimental study of different approaches for active control of sound transmission through double walls, Journal of the Acoustical Society of America 102 (3) (1997) 1664–1670.
[6] J. Pan, C. Bao, Analytical study of different approaches for active control of sound transmission through double walls, Journal of the Acoustical Society of America 103 (2) (1998) 1916–1922.
[7] P. Sas, C. Bao, F. Augusztinovicz, W. Desmet, Active control of sound transmission through a double panel partition, Journal of Sound and Vibration 180 (4) (1995) 609–625.
[8] R. Paurobally, J. Pan, C. Bao, Feedback control of noise transmission through a double-panel partition, in: Proceedings of Active 99, Vol. 1, 1999, pp. 375–386.
[9] S.J. Pietrzko, O.E. Kaiser, Experiments on active control of air-borne sound transmission through a double wall cavity, in: Proceedings of Active 99, Ft. Lauderdale, FL, USA, 1999.
[10] O.E. Kaiser, Active Control of Sound Transmission through a Double Wall Structure, Ph.D. Thesis, Swiss Federal Institute of Technology, Zurich, 2001.
[11] F. Fahy, Sound and Structural Vibration: Radiation, Transmission and Response, Academic Press, London, 1985.
[12] C.R. Fuller, S.J. Elliott, P.A. Nelson, Active Control of Vibration, Academic Press, London, 1996.
[13] J.E. Lagnese, G. Leugering, Controllability of thin elastic beams and plates, in: The Control Handbook, CRC Press, IEEE Press, Boca Raton, FL, New York, 1996, pp. 1139–1156.
[14] L.L. Beranek, I.L. Vér (Eds.), Noise and Vibration Control Engineering, Principles and Application, Wiley, New York, 1992.
[15] L.L. Beranek, Acoustics, McGraw-Hill, New York, 1954.
[16] P.A. Nelson, S.J. Elliott, Active Control of Sound, (3rd Printing), Academic Press, London, 1995.
[17] S.J. Elliott, M.E. Johnson, Radiation modes and the active control of sound power, Journal of the Acoustical Society of America 94 (4) (1993) 2194–2204.
[18] W.T. Baumann, W.R. Saunders, H.H. Robertshaw, Active suppression of acoustic radiation from impulsively excited structures, Journal of the Acoustical Society of America 90 (6) (1991) 3202–3208.
[19] D.R. Thomas, P.A. Nelson, Feedback control of sound radiation from a plate excited by a turbulant boundary layer, Journal of the Acoustical Society of America 98 (5) (1995) 2651–2662.
[20] W. Gawronski, Actuator and sensor placement for structural testing and control, Journal of Sound and Vibration 208 (1) (1997) 101–109.
[21] J.C. Doyle, B.A. Francis, A.R. Tannenbaum, Feedback Control Theory, Macmillan, New York, 1992.
[22] R.L. Clark, Adaptive structures: compensators by design, in: Proceedings of Active 99, Vol. 1, 1999, pp. 63–72.
[23] O.E. Kaiser, A.A. Julius, S.J. Pietrzko, M. Morari, Uncontrollable modes in double wall panels, in: Proceedings of International Congress on Acoustics, Rome, 2001.
[24] K. Zhou, J.C. Doyle, K. Glover, Robust and Optimal Control, Prentice-Hall, Englewood Cliffs, NJ, 1996.
[25] G.J. Balas, J.C. Doyle, K. Glover, A. Packard, R. Smith, $\mu$-Analysis and Synthesis Toolbox User's Guide: For Use with MATLAB, The MathWorks Inc., Natick, MA, 1995.
[26] M. Morari, E. Zafiriou, Robust Process Control, Prentice-Hall, Englewood Cliffs, NJ, 1989.
[27] S. Prajna, O.E. Kaiser, S.J. Pietrzko, M. Morari, Robust active control of a vibrating plate, in: Proceedings of Noise Con 2000, New Port Beach, CA, 2000.
[28] P. van Overschee, B. De Moor, Subspace Identification for Linear Systems, Kluwer Academic Publishers, Dordrecht, 1996.
[29] A.V. Oppenheim, R.W. Schafer, Discrete-Time Signal Processing, Prentice-Hall, Englewood Cliffs, NJ, 1989.
[30] L. Ljung, System Identification Toolbox User's Guide: For Use with MATLAB, The MathWorks Inc., Natick, MA, 1991.

[31] O.E. Kaiser, R. Pfiffner, Modeling and robust control of active noise control systems, IfA-Report AUT 96-09, Automatic Control Laboratory, Swiss Federal Institute of Technology, Zurich, 1996.
[32] O.E. Kaiser, R. Pfiffner, M.V. Kothare, F.J. Kraus, C. Rhodes, M. Morari, Modeling and robust control of active noise control systems, in: Proceedings of the IEEE Conference on Decision and Control, Vol. 3, Kobe, Japan, 1996, pp. 2771–2772.
[33] R.S. Smith, Eigenvalue perturbation models for robust control, IEEE Transactions on Automatic Control 40 (1995) 1063–1066.